Operando infrared spectroscopy study of iron-catalyzed hydromagnesiation of styrene: Explanation of non-linear catalyst and inhibitory substrate dependencies

Jessica A. Rogers and Brian V. Popp*

C. Eugene Bennett Department of Chemistry, West Virginia University, Morgantown, West Virginia, USA.

KEYWORDS: iron-catalysis, hydromagnesiation, operando spectroscopy, alkene functionalization, reaction mechanism

ABSTRACT: A mechanistic study of iron-catalyzed hydromagnesiation of styrene using operando infrared spectroscopy is reported. Kinetic investigation by both initial and observed rate measurements indicate complex concentration dependencies on the iron catalyst as well as sacrificial Grignard reagent and styrene. Global numeric analysis of probable mechanisms using COmplex PAthway Simulator (COPASI) led to the identification of a twelve step mechanism that accurately reproduces experimental timecourse data over a wide variety of reaction conditions. Predictions using the hydromagnesiation mechanism reveal the origins of the observed kinetic complexity.

Over the last decade, the discovery and utilization of earth-abundant metal catalysts have transformed the field of homogeneous organometallic chemistry, enabling researchers to develop synthetic methods that rivals precious metal catalysts in terms of reaction scope, selectivity, and efficiency as well as positively impact environmental and economic sustainability.[1] Reductive functionalization reactions of alkenes have been especially prominent with important examples of hydrofunctionalization, (hydroboration,[2] hydrosilylation,[3] hetero(element)-functionalization[4]) as well as reductive cross-coupling,[5] and hydrogenation.[6] A lesser explored class of alkene reductive functionalization proceeding through transfer hydrometallation, specifically hydromagnesiation[7] or hydrozincation,[8] have also been reported however, the catalyst systems suffer from limited substrate scope and selectivity. Nevertheless, these reactions provide access to more complex, valuable organometallic reagents that are amenable to subsequent reaction with a variety of electrophiles including CO_2, an important underutilized C_1 feedstock.[9]

While detailed mechanistic investigations have been key to elucidating the structural and electronic features of the metal catalyst. Unlike other alkene reductive functional reactions, mechanistic studies are sparse for transfer hydrometallation.[7c,10] Kochi described this class of reaction as proceeding through "the basic transformation of metal-alkyls" (Figure 1A) belying the likely mechanistic complexity often observed with reactions of organometallic reagents.[11] Only recently have significant strides been made to elucidate the mechanism of these transformations. Thomas utilized *in situ* generated catalyst, 2,6-bis[1-(2,6-diisopropylphenylimino)ethyl]pyridine iron(II)dichloride (iron-PDI), to achieve hydromagnesiation of electron-rich and neutral styrene derivatives (Figure 1B). Subsequent

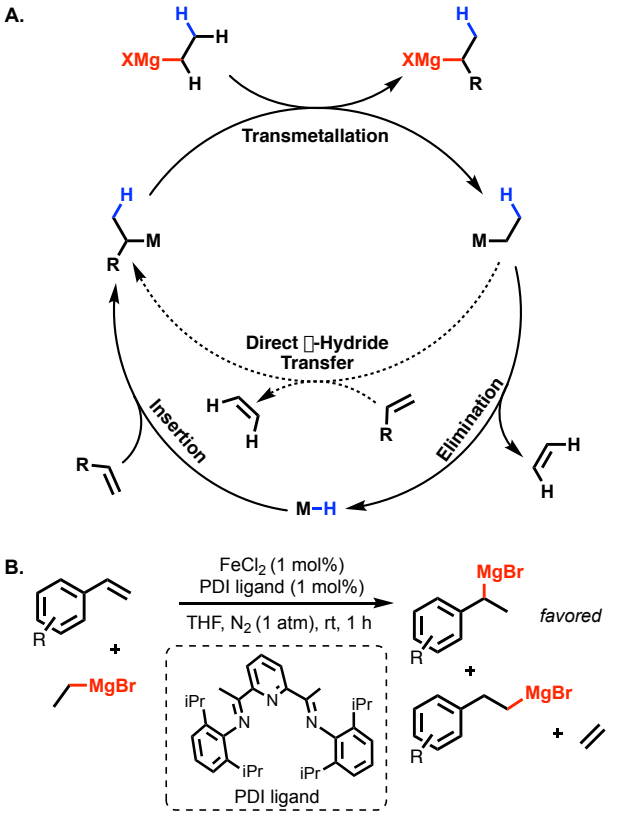

Figure 1. General mechanistic and synthetic schemes illustrating transfer hydrometallation. A) Traditionally proposed mechanism for hydromagnesiation (outer cycle). B) Thomas' hydromagnesiation of styrene derivatives.

mechanistic analysis revealed: 1) kinetic complexity arising from catalyst as well as Grignard and alkene substrates/products; 2) direct β-hydride transfer (Figure 1A), not elimination/insertion, as a likely elementary catalytic step from deuterium labeling studies; 3) formal iron(0)-ate species as comprising both resting state and off-cycle catalytic intermediates.[10c] The mechanistic investigations reported to-date have yet to define clearly the origin of the complex kinetic behavior nor do they directly take into account the role that formation of the linear Grignard product play on the overall kinetics. Herein, we utilize operando infrared spectroscopy to perform a detailed kinetic analysis and numerical modelling of the Thomas hydromagnesiation reaction that explains the kinetic complexity observed, offering a mechanistic foundation for future development of iron-catalyzed transfer hydrometallation reactions.

We initiated our studies by examining Thomas' hydromagnesiation reaction between styrene (**S**) and cyclopentylmagnesium bromide (**G**) with isolated (PDI)$FeCl_2$ pre-catalyst using a ReactIR 15 system (Figure 2). The sacrificial Grignard reagent was previously shown to lead to high yields of branched Grignard product with slightly lower regioselectivity as compared to ethylmagnesium bromide.[7g] The reagent was chosen to simplify reaction analysis due to the formation of soluble cyclopentene (**CYP**) product as compared to gaseous ethylene. Infrared spectral signatures for both branched (**BR**) and linear (**L**) products were unambiguously identified at 1590 cm^{-1} and 1602 cm^{-1}, respectively (Figure 2B), and through spectral deconvolution, reaction timecourses for both regioisomers were obtained (Figure 2C). Reaction timecourses generally exhibited approximate exponential growth of both products, allowing both initial rate and observed rate constants to be determined.

Kinetic analysis of the hydromagnesiation reaction were performed by independently varying the concentration of reactants, catalyst, and cyclopentene product. The results, as presented in Figure 3, reveal complex kinetic behavior. Specifically, analysis of initial rates indicates non-linear kinetic behavior for both catalyst and Grignard reagent while linear behavior, which does not proceed through the origin, was observed for styrene. Analysis of observed rates reveal linear kinetic behavior for catalyst

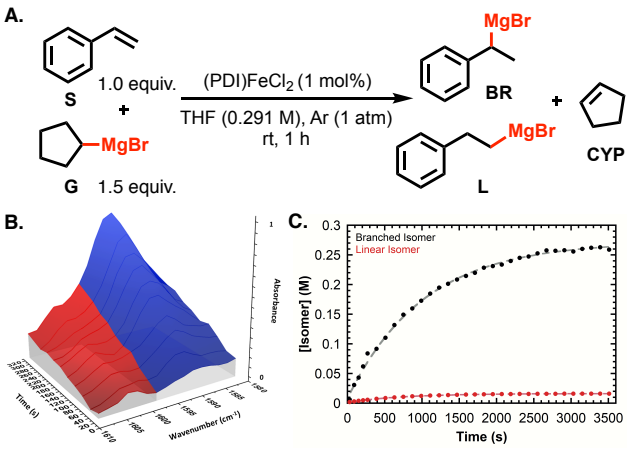

Figure 2. Standard hydromagnesiation reaction conditions (A) and representative depictions of operando infrared spectroscopy timecourse data (B-C).

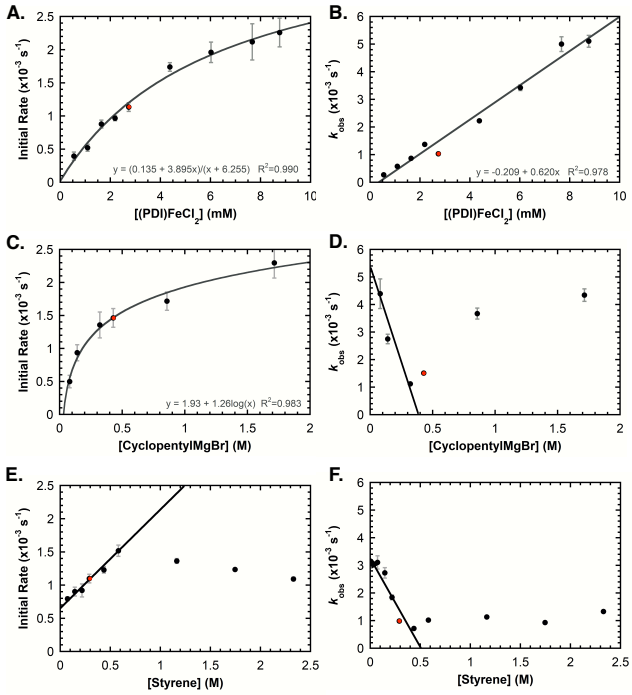

Figure 3. Concentration dependencies of initial and observed rates for catalyst and substrates. Points in red represent standard reaction conditions (see Figure 2).

and inhibitory behavior at low concentration for both Grignard reagent and styrene. When the concentrations of the substrates are similar or in excess, the behavior changes with Grignard displaying increasing non-linear kinetic behavior and styrene displaying no change in rate. This suggests that transmetallation to form the new Grignard product is the turnover limiting step, which is consistent with studies by Thomas.[7g,10c] Addition of exogenous cyclopentene, up to 15 equivalents relative to styrene, shows no effect on initial rate or observed rate (Figure S6).

Given the complexity of the kinetic behavior, COmplex PAthway Simulator (COPASI) was used for global numeric analysis of probable mechanisms of transfer hydrometallation.[12] Parameter estimations and LSODA deterministic timecourse analysis allowed for comparison to experimentally collected timecourses. A collection of ten timecourses were chosen to reflect various experimental regimes and used for global numeric fitting.[13] We first analyzed the two minimalistic mechanisms suggested by Kochi and Thomas β-hydride elimination/migratory insertion (BHE/MI) and direct β-hydride transfer (DHT), respectively (Figure 1A). Poor agreement with experimental timecourses was noted for nearly all COPASI-estimated timecourses based on simple iron(II) BHE/MI and DHT mechanisms as well as the formal iron(0) mechanism recently forwarded by Thomas and Neidig (c.f., Scheme S1 and Figure S13).[10c] This result was not surprising given the non-linearity of catalyst and Grignard initial rates data. The former data set (Figure 3A) fit best to a hyperbolic function, potentially suggesting bimolecular catalyst decomposition,[14] while the latter data set (Figure 3C) displayed apparent saturation behavior based on Lineweaver-Burk analysis (Figure S10). Both of these mechanistic steps appeared reasonable based on reported bimolecular reactions of (PDI)$FeCl_2$,[15] and by analogy

to proposed organoaluminum complexation with PDI-iron ethylene polymerization catalysts.[16] Unfortunately, poor agreement was observed when different variations of these elementary steps were included and numerically simulated.[17]

We eventually arrived at a collection of twelve elementary reactions (Figure 4) that yielded excellent agreement with the representative timecourses by sequentially assessing the mechanistic impact of three kinetic observations:[18] 1) linear initial rate dependence with a non-zero intercept for styrene (Figure 3E); 2) inhibitory behavior of both styrene and Grignard at low concentrations; 3) varying amounts of Grignard product, **L,** depending on reaction conditions;. The initial rate dependence of styrene suggested strongly that a facile styrene-promoted precatalyst activation pathway exists (Step 1A-2B) that outcompetes unaided Grignard activation (Step 1-2). Such behavior is well-known in enzyme kinetic studies to lead to hyperbolic catalyst dependencies.[19]

In an attempt to explain the inhibitory behavior of styrene at low concentrations, we introduced a reversible pathway by which the catalytic species $\mathbf{III^{BR}}$ preceding the TLS may be trapped off-cycle (Step 8). The resulting COPASI timecourse analysis, with all elementary steps set as reversible, yielded excellent agreement over the entire timecourse collection, Scheme S7 and Figure S24-25. Introduction of a similar off-cycle species from $\mathbf{III^{L}}$ led to poorer agreement with experimental data. Importantly, all attempts to identify a mechanism in which an Fe-H intermediate (ie., BHE/MI pathway) was kinetically relevant were unsuccessful, corroborating Thomas' proposal that this hydromagnesiation proceeds through a DHT pathway.

Thomas noted that linear Grignard, **L**, isomerized to branched Grignard, **BR**, in the presence of alkene and iron catalyst.[7g,10a,c] We monitored the isomerization reaction in the presence of styrene (10 mol% and 100 mol%) by *in situ* IR spectroscopy and the observed rate of isomerization was calculated to be only a single order of magnitude slower than the observed rate of hydromagnesiation (Figure S12), implying that the isomerization process (Step 7 and 9) may be kinetically relevant under certain reaction regimes. Upon introduction of these new steps, poorer agreement was observed when all elementary steps were set as reversible. Recognizing that previous mechanistic work with EtMgBr led to the conclusion that formation of both intermediate $\mathbf{III^{BR}}$ and product **BR** were irreversible, Steps 4–6 were also evaluated as irreversible as shown in Figure 4. The resulting kinetic model exhibited excellent agreement over all timecourses collected (24 data sets), Figures S26-28. The kinetic model was then used to predict, with good agreement, timecourse data for a reaction in which regioselectivity is initially poor but improves steadily over time as observed previously by Thomas (Figure S28).[7g]

Explanations for the complex observed kinetic dependencies were sought by simulating timecourse data under various regimes using the collection of elementary steps and rate constants. When the concentration of catalyst was varied at a higher concentration of Grignard substrate (3 equiv), the non-linear catalyst dependence became linear. Gratifyingly, these results were corroborated experimentally (Figure S29). Further,

A.

#	Elementary Step	k_{for} (s^{-1})	k_{rev} (s^{-1})	K_{eq}
1A	I + S ⇌ I•S	3.99E+4	1.76	2.27E+4
2A	I•S + G ⇌ I•S•G	262.6	0.083	3.16E+3
2B	I•S•G ⇌ II•S	5.45E+4	1.28E-4	4.26E+8
1	I + G ⇌ I•G	5.83	4.42E+3	1.32E-3
2	I•G ⇌ II	68.7	0.53	129.6
3	II + S ⇌ II•S	1.37	0.29	4.72
4	II•S → $\mathbf{III^{BR}}$ + CYP	1.35	---	---
5	$\mathbf{III^{BR}}$ + G → II + BR	1.41	---	---
6	II•S → $\mathbf{III^{L}}$ + CYP	0.22	---	---
7	$\mathbf{III^{L}}$ + G ⇌ II + L	0.39	43.74	8.92E-3
8	$\mathbf{III^{BR}}$ + S → $\mathbf{III^{BR}}$•S	0.0072	2.03E-4	35.5
9	$\mathbf{III^{L}}$ + S ⇌ $\mathbf{III^{BR}}$ + S	0.0084	---	---

B.

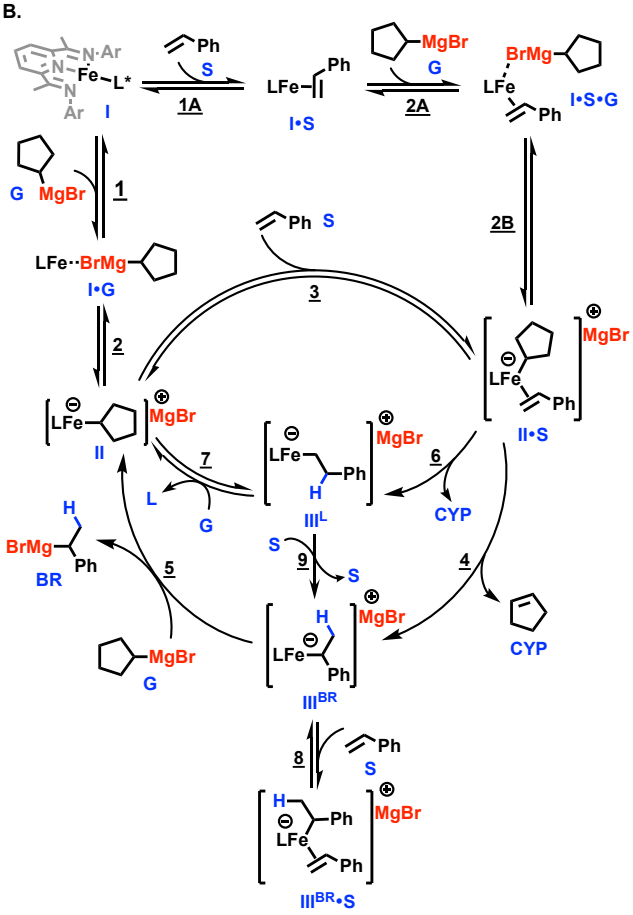

Figure 4. Proposed mechanism of transfer hydromagnesiation based upon global numerical modelling (L = PDI, L = Linear isomer).

when the model was altered such that Step 7 (ie., transmetallation to form **L**) was irreversible, the catalyst dependence also became linear (Figure S30), strongly suggesting that the hyperbolic catalyst dependence, measured by initial rates, is a consequence of kinetically complex interplay between active catalyst and linear Grignard product as catalyst loading increases.

Through similar timecourse simulations, specifically the removal of Steps 6-9 (ie., formation of linear Grignard **L** and trapping iron catalyst off-cycle $\mathbf{III^{BR}}$•**S**), we found observed rate vs. concentration behavior that no longer qualitatively mirrored the experimentally observed inhibitory behavior of Grignard and styrene substrates at low concentration (Figure S31-32). The absence of agreement implies that kinetic formation of off-cycle intermediate, $\mathbf{III^{BR}}$•**S**, and linear Grignard, **L**, are integrally

linked to the inhibitory behavior. This may suggest that Grignard isomerization processes play a key role in the substrate dependence kinetics.

Finally, we applied the kinetic model in Figure 4B to Thomas' 2012 reported reaction timecourse using ethylmagnesium bromide, under an N_2 gas.[7g,10c] The predicted timecourse fits the data remarkably well (Figure S33) given that off-cycle low valent iron-dinitrogen species were observed and characterized by Thomas/Neidig (Scheme S1).[10c] This demonstrates the likelihood that this kinetic model provides a mechanistic foundation by which similar transfer hydrometallation reactions with different Grignard reagents or alkene derivatives can be understood.[20]

The collection of elementary steps is depicted in a concise mechanism in Figure 4B. Based upon recent work by Chirik and Thomas/Neidig, formal (PDI)iron(0) species result rapidly upon treatment of iron(II) pre-catalyst with >20 equiv. of Grignard reagent.[21] Thus, we believe that a formal iron(0) species **I**, ligated by cyclopentene or solvent, enters the catalytic cycle through competing pathways in which ligand substitution occurs with either an equivalent of Grignard reagent, under limiting styrene conditions, to form first an adduct **I•G** that enters the catalytic cycle as iron-alkyl **II**, or styrene yields **I•S** that subsequently undergoes transmetallation and enters the catalytic cycle as styrene-bound iron-alkyl **II•S**. The role of vinyl arene to activate the pre-catalyst may be a critical design feature to consider in future catalyst optimization studies and may contribute to substrate scope limitations in this catalytic system. Intermediate **II•S** undergoes competing 2,1- and 1,2-insertion pathways to yield iron-benzyl, $\mathbf{III^{BR}}$, and iron-homobenzyl, $\mathbf{III^{L}}$. The rate constants for the forward reactions indicate approximately 6.1-fold faster formation of $\mathbf{III^{BR}}$. The irreversibility of steps 4, 6, and 9 is consistent with experimental observations made with cyclopentene and other disubstituted alkenes by Thomas.[10a,c] Transmetallation of $\mathbf{III^{BR}}$ is favored over $\mathbf{III^{L}}$, the reversibility of $\mathbf{III^{L}}$ leads to the probability of isomerization to $\mathbf{III^{BR}}$ in the presence of excess styrene. The irreversibility of Step 5, transmetallation of $\mathbf{III^{BR}}$, is consistent with previous deuterium studies discussed by Thomas, wherein branched Grignard product does not reenter the catalytic cycle.[7g,10a,c] Finally, $\mathbf{III^{BR}}$ may react with another equivalent of styrene to form off-cycle alkene adduct $\mathbf{III^{BR}}$**•S**. Conceivably, such a species would be necessary to access the catalytically competent off-cycle (η^2-styrene)$_3$Fe^0(benzyl) anion intermediate identified and independently prepared by Thomas and Neidig.[10c] Notably, their study showed that this species accounted for only a small percentage of catalytically active iron at early time points then increased steadily over the course of the reaction.[10c] This observed catalyst decomposition behavior is consistent with approx. 10^3 slower formation of $\mathbf{III^{BR}}$**•S** relative to formation of branched Grignard product via transmetallation (Step 5).

In summary, we have carried out a mechanistic study of an underutilized class of alkene hydrofunctionalization reaction, transfer hydrometallation. Using *in situ* infrared spectroscopic studies and global numeric modeling, a detailed understanding of the kinetic complexities of hydromagnesiation of styrene by iron-PDI catalyst has been reached. In future work, we hope to identify the electronic/steric features of the sacrificial organometallic reductant and alkene substrate that lead to efficient and selective catalysis. We anticipate that this work will provide an important foundation by which rationale earth abundant catalyst design can be achieved for this and similar reductive functionalization reactions.

ASSOCIATED CONTENT

Supporting Information:

Full experimental procedures, kinetics data, and numerical simulation results. This material is available free of charge via the Internet at http://pubs.acs.org.

AUTHOR INFORMATION

Corresponding Author

* Brian V. Popp: Brian.Popp@mail.wvu.edu

Funding Sources

This research was supported by a National Science Foundation (NSF) Career Award (CHE-1752986), NSF-MRI Award (CHE-1427136), and an ACS-PRF Grant (ACS-PRF 53298-DNI3).

Notes

The authors declare no competing financial interests.

ACKNOWLEDGMENT

We would like to thank Dr. Trina Perrone and Leandra Forte for their assistance with initial operando infrared spectroscopy experiments. We are also grateful to Prof. Fabian Goulay, Yoon Lee, and Dave Mersing for assistance with data analysis and global numerical modeling.

REFERENCES

[1] a) Su, B.; Cao, Z.-C.; Shi, Z.-J. Exploration of Earth-Abundant Transition Metals (Fe, Co, and Ni) as Catalysts in Unreactive Chemical Bond Activations. *Acc. Chem. Res.* **2015**, *48*, 886–896. b) Obligacion, J. V.; Chirik, P. J. Earth-Abundant Transition Metal Catalysts for Alkene Hydrosilylation and Hydroboration. *Nature Rev. Chem.* **2018**, *2*, 15-34. c) *Hydrofunctionalization*; Ananikov, V. P., Tanaka, M., Abbiati, G., Eds.; Topics in Organometallic Chemistry; Springer: Berlin, 2013. d) Carney, J. R.; Dillon, B. R.; Campbell, L.; Thomas, S. P. Manganese-Catalyzed Hydrofunctionalization of Alkenes. *Angew. Chem. Int. Ed.* **2018**, *57*, 10620–10624. e) Bauer, I.; Knölker, H.-J. Iron Catalysis in Organic Synthesis. *Chem. Rev.* **2015**, *115*, 3170–3387. f) *Iron Catalysis II*; Springer Berlin Heidelberg: New York, NY, **2015.** g) Pellissier, H. Recent Developments in Enantioselective Iron-Catalyzed Transformations. *Coord. Chem. Rev.* **2019**, *386*, 1–31.

[2] a) Greenhalgh, M. D.; Thomas, S. P. Chemo-, Regio-, and Stereoselective Iron-Catalysed Hydroboration of Alkenes and Alkynes. *Chem. Commun.* **2013**, *49*, 11230–11232. b) Liu, Y.; Zhou, Y.; Wang, H.; Qu, J. $FeCl_2$-Catalyzed Hydroboration of Aryl Alkenes with Bis(Pinacolato)Diboron. *RSC Adv.* **2015**, *5*, 73705–73713. c) Iwamoto, H.; Kubota, K.; Ito, H. Highly Selective Markovnikov Hydroboration of Alkyl-Substituted Terminal Alkenes with a Phosphine–Copper(I) Catalyst. *Chem. Commun.* **2016**, *52*, 5916–5919. d) Agahi, R.; Challinor, A. J.; Carter, N. B.; Thomas, S. P. Earth-Abundant Metal Catalysis Enabled by Counterion Activation. *Org. Lett.* **2019**, *21*, 993–997.

[3] a) Archer, A. M.; Bouwkamp, M. W.; Cortez, M.-P.; Lobkovsky, E.; Chirik, P. J. Arene Coordination in Bis(Imino)Pyridine Iron Complexes: Identification of Catalyst Deactivation Pathways in Iron-Catalyzed Hydrogenation and Hydrosilation. *Organometallics* **2006**, *25*, 4269–4278 b) Tondreau, A. M.; Atienza, C. C. H.; Darmon, J. M.; Milsmann, C.; Hoyt, H. M.; Weller, K. J.; Nye, S.

A.; Lewis, K. M.; Boyer, J.; Delis, J. G. P.; et al. Synthesis, Electronic Structure, and Alkene Hydrosilylation Activity of Terpyridine and Bis(Imino)Pyridine Iron Dialkyl Complexes. *Organometallics* **2012**, *31*, 4886–4893. c) Greenhalgh, M. D.; Frank, D. J.; Thomas, S. P. Iron-Catalysed Chemo-, Regio-, and Stereoselective Hydrosilylation of Alkenes and Alkynes Using a Bench-Stable Iron(II) Pre-Catalyst. *Adv. Synth. Catal.* **2014**, *356*, 584–590.

[4] a) Butcher, T. W.; McClain, E. J.; Hamilton, T. G.; Perrone, T. M.; Kroner, K. M.; Donohoe, G. C.; Akhmedov, N. G.; Petersen, J. L.; Popp, B. V. Regioselective Copper-Catalyzed Boracarboxylation of Vinyl Arenes. *Org. Lett.* **2016**, *18*, 6428–6431. b) Li, S.; Ma, S. Quadri-Synergetic Effect for Highly Effective Carbon Dioxide Fixation and Its Application to Indoloquinolinone. *Adv. Synth. Catal.* **2012**, *354*, 2387–2394. c) Fujihara, T.; Tani, Y.; Semba, K.; Terao, J.; Tsuji, Y. Copper-Catalyzed Silacarboxylation of Internal Alkynes by Employing Carbon Dioxide and Silylboranes. *Angew. Chem. Int. Ed.* **2012**, *51*, 11487–11490. d) Miao, B.; Li, S.; Li, G.; Ma, S. Cyclic Anti-Azacarboxylation of 2-Alkynylanilines with Carbon Dioxide. *Org. Lett.* **2016**, *18*, 2556–2559.

[5] a) Bedford, R. B. How Low Does Iron Go? Chasing the Active Species in Fe-Catalyzed Cross-Coupling Reactions. *Acc. Chem. Res.* **2015**, *48*, 1485–1493. b) Bauer, G.; Wodrich, M. D.; Scopelliti, R.; Hu, X. Iron Pincer Complexes as Catalysts and Intermediates in Alkyl–Aryl Kumada Coupling Reactions. *Organometallics* **2015**, *34*, 289–298. c) Thompson, C. V.; Davis, I.; DeGayner, J. A.; Arman, H. D.; Tonzetich, Z. J. Iron Pincer Complexes Incorporating Bipyridine: A Strategy for Stabilization of Reactive Species. *Organometallics* **2017**, *36*, 4928–4935. d) Sears, J. D.; Neate, P. G. N.; Neidig, M. L. Intermediates and Mechanism in Iron-Catalyzed Cross-Coupling. *J. Am. Chem. Soc.* **2018**, *140*, 11872–11883.

[6] a) Chirik, P. J. Iron- and Cobalt-Catalyzed Alkene Hydrogenation: Catalysis with Both Redox-Active and Strong Field Ligands. *Acc. Chem. Res*. **2015**, *48*, 1687–1695. b) Zell, T.; Milstein, D. Hydrogenation and Dehydrogenation Iron Pincer Catalysts Capable of Metal–Ligand Cooperation by Aromatization/Dearomatization. *Acc. Chem. Res*. **2015**, *48*, 1979–1994.

[7] a) Finkbeiner, H.; Cooper, G. Titanium-Catalyzed Isomerization and Olefin-Exchange Reactions of Alkylmagnesium Halides: A Novel Method for Preparation of the Grignard Reagent. *J. Am. Chem. Soc.* **1961**, *26*, 4779–4780. b) Tamura, M.; Kochi, J. K. Vinylation of Grignard Reagents. Catalysis by Iron. *J. Am. Chem. Soc.* **1971**, *93*, 1487–1489. c) Smith, R. S.; Kochi, J. K. Mechanistic Studies of Iron Catalysis in the Cross Coupling of Alkenyl Halides and Grignard Reagents. *J. Org. Chem.* **1976**, *41*, 502–509. d) Sato, F.; Urabe, H. Hydromagnesiation of Alkenes and Alkynes. In *Grignard Reagents: New Developments*; Wiley, **2000**; pp 65–105. e) Shirakawa, E.; Ikeda, D.; Yamaguchi, S.; Hayashi, T. Fe–Cu Cooperative Catalysis in the Isomerization of Alkyl Grignard Reagents. *Chem. Commun.* **2008**, 10, 1214-1215. f) Shirakawa, E.; Ikeda, D.; Masui, S.; Yoshida, M.; Hayashi, T. Iron–Copper Cooperative Catalysis in the Reactions of Alkyl Grignard Reagents: Exchange Reaction with Alkenes and Carbometalation of Alkynes. *J. Am. Chem. Soc.* **2012**, *134*, 272–279. g) Greenhalgh, M. D.; Thomas, S. P. Iron-Catalyzed, Highly Regioselective Synthesis of α-Aryl Carboxylic Acids from Styrene Derivatives and CO_2. *J. Am. Chem. Soc.* **2012**, *134*, 11900–11903. h) Greenhalgh, M. D.; Kolodziej, A.; Sinclair, F.; Thomas, S. P. Iron-Catalyzed Hydromagnesiation: Synthesis and Characterization of Benzylic Grignard Reagent Intermediate and Application in the Synthesis of Ibuprofen. *Organometallics* **2014**, *33*, 5811–5819. i) Shao, P.; Wang, S.; Chen, C.; Xi, C. Cp_2TiCl_2 -Catalyzed Regioselective Hydrocarboxylation of Alkenes with CO_2. *Org. Lett.* **2016**, *18*, 2050–2053.

[8] a) Gao, Y.; Urabe, H.; Sato, F. First Practical Hydrozincation of Dienes Catalyzed by Cp_2TiCl_2. Generation of Allylzinc Reagent and Its Reaction with Carbonyl Compounds. *J. Org. Chem.* **1994**, *59*, 5521–5523. b) Gao, Y.; Harada, K.; Hata, T.; Urabe, H.; Sato, F. Stereo- and Regioselective Generation of Alkenylzinc Reagents via Titanium-Catalyzed Hydrozincation of Internal Acetylenes. *J. Org. Chem.* **1995**, *60*, 290–291. c) Klement, I.; Lütjens, H.; Knochel, P. Oxidation of Zinc Organometallics Prepared by Hydrozincation or Carbozincation Using Oxygen. *Tet. Lett.* **1995**, *36*, 3161–3164. d) Vettel, S.; Vaupel, A.; Knochel, P. A New Preparation of Diorganozincs from Olefins via a Nickel Catalyzed Hydrozincation. *Tet. Lett.* **1995**, *36*, 1023–1026. e) Williams, C. M.; Johnson, J. B.; Rovis, T. Nickel-Catalyzed Reductive Carboxylation of Styrenes Using CO_2. *J. Am. Chem. Soc*. **2008**, *130*, 14936–14937.

[9] Jones, A. S.; Paliga, J. F.; Greenhalgh, M. D.; Quibell, J. M.; Steven, A.; Thomas, S. P. Broad Scope Hydrofunctionalization of Styrene Derivatives Using Iron-Catalyzed Hydromagnesiation. *Org. Lett.* **2014**, *16*, 5964–5967.

[10] a) Greenhalgh, M. *Iron-Catalysed Hydrofunctionalisation of Alkenes and Alkynes*; Springer Theses; Springer International Publishing: Cham, 2016. b) Ren, Q.; Wu, N.; Cai, Y.; Fang, J. DFT Study of the Mechanisms of Iron-Catalyzed Regioselective Synthesis of α-Aryl Carboxylic Acids from Styrene Derivatives and CO_2. *Organometallics* **2016**, *35*, 3932–3938 c) Neate, P.; Greenhalgh, M. D.; Brennessel, W. W.; Thomas, S. P.; Neidig, M. L. Mechanism of the Bis(Imino)Pyridine Iron-Catalyzed Hydromagnesiation of Styrene Derivatives. *J. Am. Chem. Soc.* **2019**, *141*, 10099-10108.

[11] Kochi, J. K. Organometallic Mechanisms and Catalysis, 1st Ed.; Academic Press, 1978, pg. 380-381.

[12] Hoops, S.; Gauges, R.; Lee, C.; Pahle, J.; Simus, N.; Singhal, M.; Xu, L.; Mendes, P.; Kummer, U. COPASI - A COmplex PAthway SImulator. *Bioinformatics* **2006**, 22, 3067–3074.

[13] See Supporting Information for full details on numeric modelling and use of Cohen's κ for assessing agreement between numerical and experimental timecourses..

[14] For notable examples that illustrate this kinetic behavior, see: a) Bakac, A.; Won, T.-J.; Espenson, J. H. Novel Pathways in the Reactions of Superoxometal Compounds. *Inorg. Chem.* **1996**, *35*, 2171. b) Steinhoff, B. A.; Guzei, I. A.; Stahl, S. S. Mechanistic Characterization of Aerobic Alcohol Oxidation Catalyzed by Pd(OAc)2/Pyridine Including Identification of the Catalyst Resting State and the Origin of Nonlinear [Catalyst] Dependence. *J. Am. Chem. Soc.* **2004**, 126, 11268–11278.

[15] a) Wile, B. M.; Trovitch, R. J.; Bart, S. C.; Tondreau, A. M.; Lobkovsky, E.; Milsmann, C.; Bill, E.; Wieghardt, K.; Chirik, P. J. Reduction Chemistry of Aryl- and Alkyl-Substituted Bis(Imino)Pyridine Iron Dihalide Compounds: Molecular and Electronic Structures of [$(PDI)_2$Fe] Derivatives. *Inorg. Chem.* **2009**, 48, 4190–4200. b) Shejwalkar, P.; Rath, N. P.; Bauer, E. B. New Bis(Imino)Pyridine Complexes of Iron(II) and Iron(III), and Their Catalytic Activity in the Mukaiyama Aldol Reaction. *Synthesis* **2014**, *46*, 57–66.

[16] Tondreau, A. M.; Milsmann, C.; Patrick, A. D.; Hoyt, H. M.; Lobkovsky, E.; Wieghardt, K.; Chirik, P. J. Synthesis and Electronic Structure of Cationic, Neutral, and Anionic Bis(Imino)Pyridine Iron Alkyl Complexes: Evaluation of Redox Activity in Single-Component Ethylene Polymerization Catalysts. *J. Am. Chem. Soc.* **2010**, *132* (42), 15046–15059.

[17] See Schemes S2-3 and accompanying data in the Supporting Information.

[18] The mechanism in Figure 4 arose by iterative introduction of elementary steps to explain observed complex kinetic behavior, see Schemes S4-6 in the Supporting Information.

[19] Cornish-Bowden, A. *Principles of Enzyme Kinetics*; Elsevier, 2014.

[20] Catalytically competent low valent iron species resulting from decomposition of PDI-iron active catalyst were not considered in the kinetic modelling. Deviation from agreement with experimental data may reflect the contribution of secondary catalytic pathways not accounted for in the proposed mechanism in Figure 4.

[21] a) Bart, S. C.; Lobkovsky, E.; Chirik, P. J. Preparation and Molecular and Electronic Structures of Iron(0) Dinitrogen and Silane Complexes and Their Application to Catalytic Hydrogenation and Hydrosilation. *J. Am. Chem. Soc.* **2004**, *126* (42), 13794–13807. b) Bart, S. C.; Chłopek, K.; Bill, E.; Bouwkamp, M. W.; Lobkovsky, E.; Neese, F.; Wieghardt, K.; Chirik, P. J. Electronic Structure of Bis(Imino)Pyridine Iron Dichloride, Monochloride, and Neutral Ligand Complexes: A Combined Structural, Spectroscopic, and Computational Study. *J. Am. Chem. Soc.* **2006**, *128* (42), 13901–13912. c) Tondreau, A. M.; Stieber, S. C. E.; Milsmann, C.; Lobkovsky, E.; Weyhermüller, T.; Semproni, S. P.; Chirik, P. J. Oxidation and Reduction of Bis(Imino)Pyridine Iron Dinitrogen Complexes: Evidence for Formation of a Chelate Trianion. *Inorg. Chem.* **2013**, *52* (2), 635–646. d) Casitas, A.; Krause, H.; Goddard, R.; Fürstner, A. Elementary Steps of Iron Catalysis: Exploring the Links between Iron Alkyl and Iron Olefin Complexes for Their Relevance in C-H Activation and C-C Bond Formation. *Angew. Chem. Int. Ed.* **2015**, *54* (5), 1521–1526. e) Yu, Y.; Smith, J. M.; Flaschenriem, C. J.; Holland, P. L. Binding Affinity of Alkynes and Alkenes to Low-Coordinate Iron. *Inorg. Chem.* **2006**, *45* (15), 5742–5751.